

VIP

Bio-orthogonal AIE Dots Based on Polyynes-Bridged Red-emissive AIEgen for Tumor Metabolic Labeling and Targeted Imaging

SPECIAL
ISSUEPengfei Zhang⁺,^[a, c, d] Tao Jiang⁺,^[a, d, e] Yuanyuan Li⁺,^[c] Zheng Zhao,^[c] Ping Gong,^[d] Lintao Cai,^[d] Ryan T. K. Kwok,^[a, c] Jacky Wing Yip Lam,^[a, c] Xinggui Gu,^{*,[b]} and Ben Zhong Tang^{*,[a, c]}

Abstract: In this work, we aim to develop cancer cell-targeting AIE dots based on a polyynes-bridged red-emissive AIEgen, 2TPE-4E, through the combination of metabolic engineering and bio-orthogonal reactions. Azide groups on a tumor were efficiently produced by intravenous injection of Ac4ManNAz and glycol-metabolic engineering. These bio-orthogonal azide groups could facilitate the specific targeting of DBCO-AIE dots to the tumor cells undergoing metal-free click reaction in vivo. The efficiency of this targeting strategy could be further improved with the development of new bio-orthogonal chemical groups with higher reactivity and a large amount of AIEgens could be delivered to the tumor for diagnosis.

Cancer is one of the major diseases threatening human health. The implementation of sensitive and specific imaging modalities for timely cancer diagnosis and progression monitoring is of great scientific and clinical significance.^[1] Targeting against the receptors of cell surface has been a big issue for tumor-specific imaging especially. Generally, the endogenous receptors on the membrane of living cells could be visualized fluorescently by different ligands labeled with fluorophores such as aptamers, peptides, antibodies, and so on.^[2] However, these active targeting strategies suffered from rather low delivery efficiency less than 0.3% because of the insufficient receptors on cell membrane, which severely impacted the performance of fluorescent probes for in vivo imaging. Therefore, it could be highly demanded to produce adequate receptors on cancerous cells homogeneously for specific targeting in tumor.^[3]

To get a high targeting efficiency, the binding properties dependent on the optimization of the preparation and the stability of the binding motif play a crucial roles.^[4] Bio-orthogonal reaction that refers to those chemical conjugation that can be performed in complicated biological microenvironments with negligible perturbation to normal biological processes and exquisite selectivity and reliability, has been proven to be particularly beneficial to biological studies. Compared to non-covalent binding-based methods, bio-orthogonal reaction relies on the highly-specific and covalent conjugation of a fluorophore to the biological molecule of interest. Therefore, bio-orthogonal reaction enables a general and valuable toolbox to improve tumor targeting ability.^[5] Besides, insufficient endogenous receptors on cancerous cell membrane directly lead to the low selectivity.^[6] To solve this problem, an alternative strategy is to manually and homogeneously paste huge receptors on tumor cells surface by metabolic glycol-engineering, which refers to a synthetic biological approach to modify the glycans and introduce various functional units, exhibiting great potential.^[7] Additionally, it is evidenced that excess nutrient such as glucose is consumed by the tumor cells, resulting in a higher concentration of sialic acid on the cancerous cell surface. Thus, the tumor can be specially labeled functional groups through metabolic glycol-engineering.^[8] Therefore, accurate tumor-targeting imaging can realize by the combination of metabolic glycol-engineering and bio-orthogonal chemistry.^[9]

Fluorescence nanoparticle-based bioimaging systems, benefiting from non-invasive, highly-resolved and real-time fluorescence technology, have attracted much attention for tumor diagnosis.^[10] Due to the potential toxicity of inorganic nanoparticles such as quantum dots (QDs), organic fluorophore-doped nanoparticles are promising alternates for clinical biomedical

[a] Dr. P. Zhang,⁺ T. Jiang,⁺ Dr. R. T. K. Kwok, Dr. J. W. Y. Lam, Prof. B. Z. Tang
HKUST Shenzhen Research Institute
No. 9 Yuexing First RD, South Area, Hi-Tech Park
Nanshan, Shenzhen, 518057 (China)
E-mail: tangbenz@ust.hk

[b] Prof. X. Gu
Beijing Advanced Innovation Center for Soft Matter Science and Engineering
Beijing University of Chemical Technology
Beijing 100029 (China)
E-mail: guxinggui@mail.buct.edu.cn

[c] Dr. P. Zhang,⁺ Dr. Y. Li,⁺ Dr. Z. Zhao, Dr. R. T. K. Kwok, Dr. J. W. Y. Lam,
Prof. B. Z. Tang
Department of Chemistry, Hong Kong Branch of Chinese National Engineering
Research Centre for Tissue Restoration and Reconstruction
Institute for Advanced Study, Institute of Molecular Functional Materials,
State Key Laboratory of Molecular Neuroscience, Division of Life Science
Hong Kong University of Science and Technology
Clear Water Bay, Kowloon, Hong Kong (China)

[d] Dr. P. Zhang,⁺ T. Jiang,⁺ Prof. P. Gong, Prof. L. Cai
Guangdong Key Laboratory of Nanomedicine, CAS Key Laboratory of
Health Informatics, Shenzhen Bioactive Materials Engineering Lab for Medicine
Institute of Biomedicine and Biotechnology, Shenzhen Institutes of Advanced
Technology, Chinese Academy of Sciences
Shenzhen 518055 (P.R. China)

[e] T. Jiang⁺
Department of Pharmaceutical Sciences, Nanfang Hospital
Southern Medical University
1838 North Guangzhou Avenue, Guangzhou (P.R. China)

[†] These authors contributed equally to this work.

Supporting information and the ORCID identification number(s) for the author(s) of this article can be found under:
<https://doi.org/10.1002/asia.201801609>.

This manuscript is part of a special issue on aggregation-induced emission. Click here to see the Table of Contents of the special issue.

imaging, because of their facile preparation, good biocompatibility, long-circulation time, and high resistance to photobleaching in physiological surrounding.^[11] However, traditional organic fluorophores seriously suffered from the detrimental aggregation-caused quenching (ACQ), due to their tendency to aggregate in the nanoparticles when increasing the doping amount. On the contrary, luminogens with aggregation-induced emission characteristic (AIEgens) could be emissive highly in aggregation state based on the restriction of the intramolecular motions (RIM), which hold great potential for fabrication of AIE dots with low cytotoxicity and high brightness for cell imaging and tumor diagnosis.^[12] In addition, these AIE NPs are fairly photostable under laser excitation, enabling reliable long-term tracking of dynamic biological processes.

As a proof of the concept, in our work, we aim to develop cancer-targeting AIE dots through the combination of metabolic glycol-engineering and bio-orthogonal reaction. The DBCO-PEG-lipids was chosen as the coating materials to fabricate bio-orthogonal AIE dots based on the polyynyl bridged red-emissive AIEgens, 2TPE-4E.^[13] According to the previous results, 2TPE-4E featured with two tetraphenylethylene derivatives located on the terminals of polyynyl holds π - π -A structure. Different from the other D-A systems, the polyynyl bridge in 2TPE-4E could not only guarantee the conjugation of the whole π -system to endow long absorption and emission wavelengths but also avoid emission quenching caused by π - π stacking. Firstly, azide-modified sialic acids are artificially produced on cancer cell membrane by an intravenous injection of tetra-acetylated *N*-azidoacetyl-*D*-mannosamine (Ac4ManNAz) *in vivo*. Secondly, bio-orthogonal AIE dots (DBCO-AIE dots) are intravenously injected into the tumor-bearing mice, then these dots will recognize the azide-modified azide sialic acids on the surface of cancer cells and label the sialic acids by metal-free click reaction *in situ*. This strategy is expected to generate receptor-like chemical azide groups on the targeted cancer cell surface dynamically and bio-orthogonally, controlling the cancer cell-targeting ability of AIE dots.

The AIE dots were prepared by nanoprecipitation method using DSPE-PEG with (DBCO-AIE dots) and without DBCO functional group modifications as encapsulation materials (Figure 1A). Because of the hydrophilic and hydrophobic interactions, AIE-active 2TPE-4E was embedded into the hydrophobic core formed by DSPE, while DBCO groups were on the surface of the outer layer fabricated by the hydrophilic PEG segment. To target azide-labelled sialic acids with bio-orthogonal manner, DBCO was chosen as a functional group due to its selective reactivity to azide groups in mild biological media. As shown in Figure 1B,C, the absorption and emission properties of as-prepared AIE dots were then investigated in PBS buffer. The absorption maximum of as-prepared AIE dots was about 520 nm, associating with the fluorescence emission peak at 630 nm, which holds particular advantages of low excitation energy and background auto-fluorescence in complicated biological environment. The DBCO-AIE dots exhibited a large Stokes shift with the value of 110 nm, which minimized the self-absorption largely in contrast to conventional organic fluorophores. Figure 1D showed the hydrodynamic diameter of as-

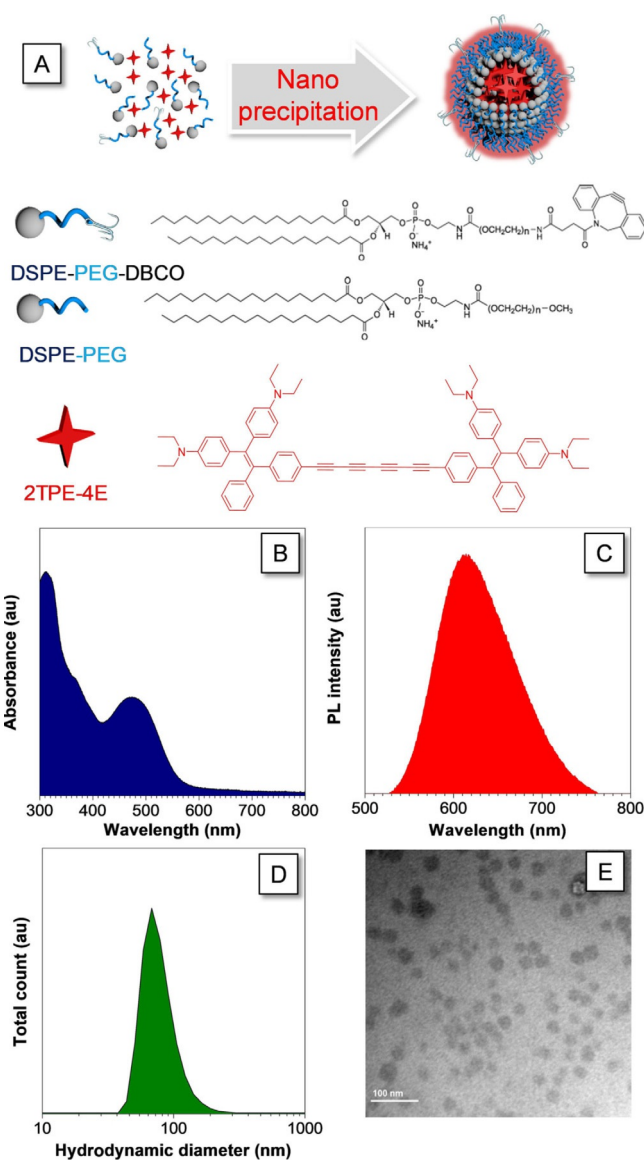


Figure 1. (A) Schematic illustration of bio-orthogonal AIE dots (DBCO-AIE dots) preparation by nanoprecipitation approach. The DBCO group on the AIE dots was used for further click chemistry reaction with azide group. Normalized absorbance (B) fluorescence spectra (C) and of DBCO-AIE dots in PBS buffer. Dynamic light scattering (DLS) diameter (D) and TEM image (E) of DBCO-AIE dots. Scale bar: 100 nm.

prepared DBCO-AIE dots, which was measured by dynamic light scattering (DLS). The results indicated the average hydrodynamic diameters of about 60 nm. Further, transmission electron microscopy (TEM) was used to study the morphology of as-prepared DBCO-AIE dots, also indicating the diameter of about 60 nm for the spherical AIE dots (Figure 1E), which was accessible for *in vivo* blood circulation. The zeta potential measurement showed that DBCO-AIE dots were negatively charged, which was ascribed to the phosphate group on DSPE-PEG (Figure S1).

Previously, it has been found that azide-modified *D*-mannosamines could be delivered into the cells and efficiently metabolized by the promiscuous sialic acid biosynthetic pathway, being incorporated into cell surface.^[9b] Thus, Ac4ManNAz, gen-

erating the artificial “receptor-like” azide group was chosen as the precursor. Moreover, previous work has shown Ac4ManNAz is very easy to enter into cells because of its four hydrophobic acyl groups, which could generate a large amount of azide groups on the surface of cells. The azido sialic acid on the surface of cell membrane were then reacted with bio-orthogonal DBCO group of AIE dots through metal-free click reaction. To investigate the cell labeling and bio-orthogonal ability of the unnatural monosaccharides and AIE dots, the human breast cancer cell lines (MCF-7) were chosen for in vitro study. For the Ac4ManNAz-treated group, the conjugation of DBCO-AIE dots to the MCF-7 cancer cells was clearly visualized by the fluorescence of 2TPE-4E under confocal laser scanning microscope (CLSM). The results indicated that there was red fluorescence with strong intensity in MCF-7 cells incubated with Ac4ManNAz, suggesting the successful metabolization of azide sialic acid. However, there were negligible fluorescence signals on the surface of the control group treated with medium without Ac4ManNAz and further addition of DBCO-AIE dots (Figure 2). Collectively, abovementioned evidently demonstrated that the azide groups could be metabolically labeled on MCF-7 cancer cells membrane by using azide-terminal tetra-acetylated acetyl-d-mannosamine in vitro. Figure 3A showed that the fluorescence of the cells enhanced with the increase of Ac4ManNAz, which indicated the number of AIE dots on the cell could be artificially controlled by variation of the amount of Ac4ManNAz in a dose-dependent manner. As shown in Figure 3B, the fluorescence also enhanced with the increase of pre-incubation time of Ac4ManNAz with MCF-7, indicating that the amount of AIE dots on MCF-7 cells could also be tuned through the time-dependent manner.

After demonstrating that azide group could be labelled on MCF-7 cells through Ac4ManNAz mediated metabolic approach and further conjugated with DBCO-AIE dots in vitro, then we investigated whether Ac4ManNAz could also label

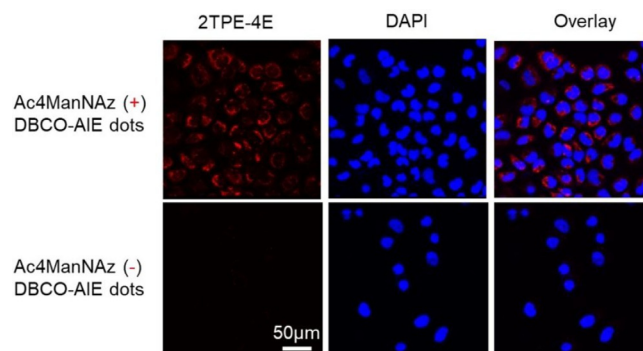


Figure 2. Metabolic labeling of MCF-7 cells in vitro with metal-free click reaction after pre-treatment of Ac4ManNAz. Confocal laser scanning microscope (CLSM) images of MCF-7 cells upon treatment with Ac4ManNAz or PBS for three days and further incubation with DBCO-AIE dots for 30 min. Cell nuclei were stained with DAPI (blue). Scale bar: 50 µm.

MCF-7 cancer cells in vivo and enhance the tumor accumulation of AIE dots (Figure 4A). The in vivo breast cancer model was established on athymic nude mice by subcutaneous injection of cancer cells in the right flank. When the size of the tumors reached $\approx 49 \text{ mm}^3$, Ac4ManNAz was intravenously injected into the mice. with once-daily manner for 4 days. 4 days later, DBCO-AIE dots were put into the mice with the manner of intravenous injection. A whole-body small-animal imaging system was utilized to image and evaluate the in vivo targeting ability of the metabolic labeling approach and in vivo distribution of DBCO-terminal AIE dots in nude mice. As displayed in Figure 4B, after injection for 6 h, the fluorescence from the Ac4ManNAz-treated group was mainly observed in the tumor area. After 12 h post-injection, the fluorescence signal became brighter. The results suggested that the fluorescence signals were only detected in the liver after injection for 0.5 h. By contrast, for mouse without injection of Ac4ManNAz, although

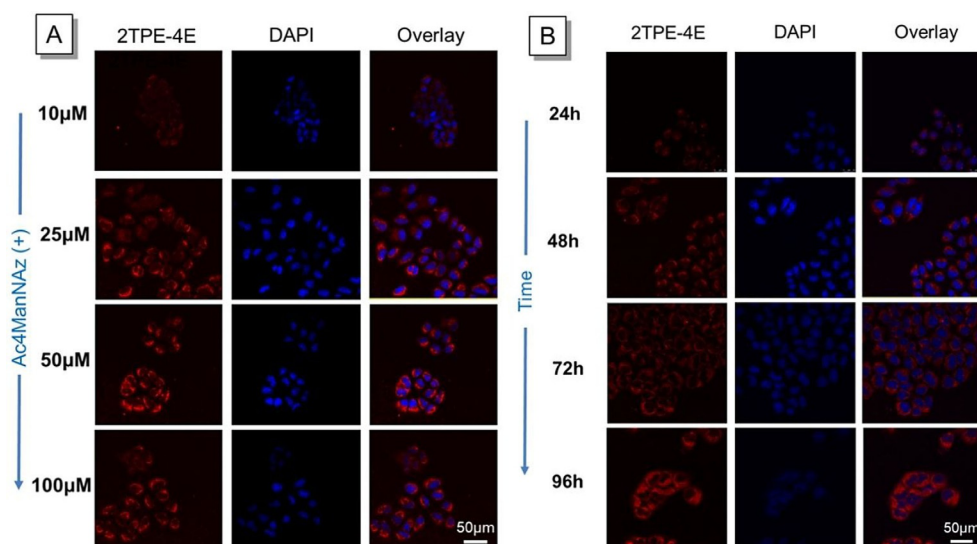


Figure 3. (A) Optimization the concentration of Ac4ManNAz for In vitro metabolic labeling of the MCF-7 cells. CLSM images of MCF-7 cells after treatment with different amount of Ac4ManNAz for three days and further incubation with DBCO-AIE dots for 30 min. (B) Optimization the incubation time of Ac4ManNAz for in vitro metabolic labeling of the MCF-7 cells. CLSM images of MCF-7 cells after treatment with Ac4ManNAz for different time and further incubation with DBCO-AIE dots for 30 min. Cell nuclei were stained with DAPI (blue). Scale bar: 50 µm.

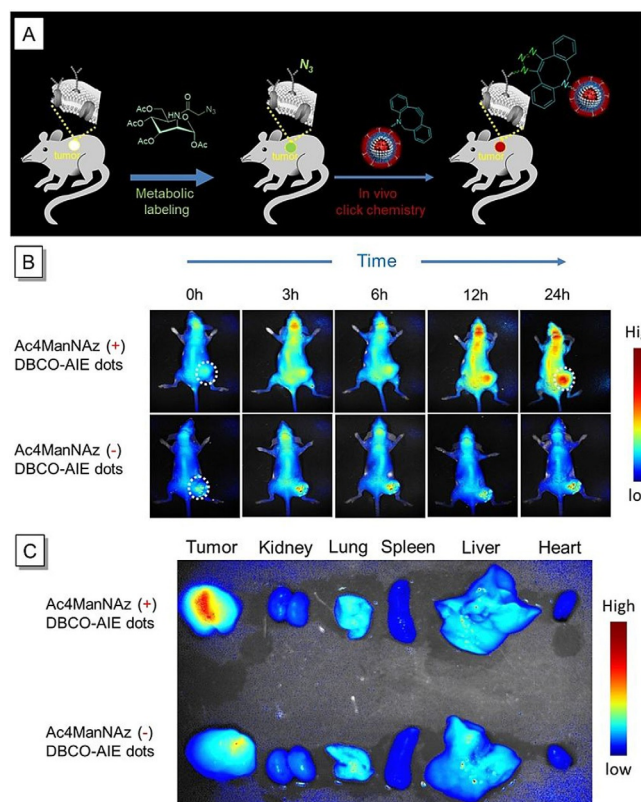


Figure 4. (A) Schematic picture of in vivo bio-orthogonal metabolic labeling of tumor by using AIE-dots. (B) In vivo imaging of metabolically labelled tumor-bearing mouse after intravenously injection of DBCO-AIE dots. The mouse without Ac4ManNAz injection was imaged as control. In vivo imaging results were taken at 0, 3, 6, 12, 24 h time point.

there was fluorescence signal all around the body and a little signal from the tumor area. However, there was little change along with the time increased to 24 h. In the end, the results showed more accumulation of AIE dots in tumor area for mouse with injection of Ac4ManNAz compared to the saline-treated group after further injection of DBCO-AIE dots.

Ex vivo imaging analysis of the main organs confirmed the excellent cancer-targeting ability of as-prepared bio-orthogonal AIE dots through the metal-free click reaction in vivo (Figure 4B). At the time point of 24 hours after injection, the main organs and tumors were dissected, and each sample was imaged by using the Maestro in vivo system. For tumor-bearing mouse, DBCO-AIE dots displayed higher fluorescent signal accumulation in tumor tissue compared to that of surrounding normal tissue due to the synergistic effect of the highly metabolic activity of tumor and the EPR (enhanced permeability and retention) effect of nanoparticles. Besides, there were also strong signal in liver and kidney as they were mainly contributed for clearance of nanomaterials. Unnatural derivatives of monosaccharides, such as the sialic acid analogue *N*-glycolylneuraminic acid, could be taken up by tissues and cells, which could be further recognized by the immune system. This kind of monosaccharide was present in all kinds of mammals and could be delivered to the cells through the digestion of dairy food supply, such as meat. It was taken up by all kinds of cells

and could be detected almost exclusively in the metabolically more active cancer cells. As a result, the signal from the tumor of the Ac4ManNAz-treated mouse is much higher than that of the mouse without treatment. All these results evidently demonstrated these AIE dots exhibited high efficiency of cancer targeting.

To study whether as-prepared bio-orthogonal DBCO-AIE dots cause in vivo side toxicity, the major organs of mice in each treatment group, such as hearts, livers, spleens, lungs and kidneys, were further excised and sectioned for the H&E staining experiment. Figure 5 suggested that almost no hydrophobic

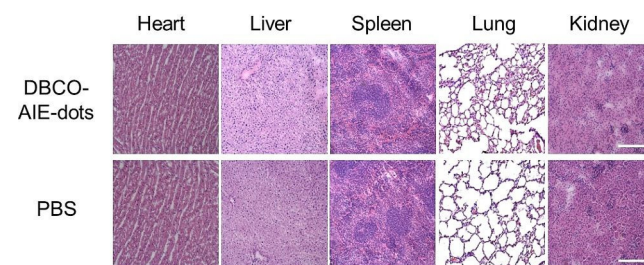


Figure 5. Representative H&E stained images of major organs including heart, liver, spleen, lung and kidney collected from the control untreated mice and DBCO-AIE-dots injected mice after 24 h injection. Almost no organ damage or lesion was detected for DBCO-AIE dots. Mice were treated with DBCO-AIE dots with dose of 5 mg kg^{-1} .

damages and lesions were detected according to these H&E stained slices after intravenously injection of DBCO-AIE dots.

In summary, we developed bio-orthogonal AIE dots based on a polyene-bridged AIEgen with red emission. Furthermore, based on these bio-orthogonal AIE dots and a metabolic glycol-engineering technique, we developed an in vivo metabolic labeling strategy for tumor-specific delivery of AIE dots and targeting imaging. The two-step signal amplification approach was performed by continuous intravenous injection of Ac4ManNAz to produce a huge amount of azide groups on the cancer cell surface to enhance the tumor-targeting ability. Secondly, DBCO-functionalized AIE-dots were put into the body through an intravenous injection of AIE dots to bio-orthogonally find and bind to the cancer cells with highly metabolic activity. Thus, various kinds of hydrophobic AIEgens could be delivered by this two-step in vivo metabolic enhanced labeling strategy. Bio-orthogonal chemistry is a powerful tool for bioprobes to be applied in labeling biological substrates. The efficiency of this technique could be further improved through developing novel bio-orthogonal reactions and functional groups with higher activity. In addition, such a bio-orthogonal metabolic enhanced approach opens a new avenue for the facile application of AIEgens to metabolic disease diagnosis and therapy. We believe these general bio-orthogonal labeling approaches based on the metabolic glycol-engineering technique provide excellent opportunities for the applications of AIE-based materials in the field of synthetic biology and hold great potential for further biomedical applications.

Acknowledgements

We are grateful for financial support from the National Science Foundation of China (21702016, 81501591, 21788102, 21490570 and 21490574), Science and Technology Plan of Shenzhen (JCYJ20170307173739739 and JCYJ20160229205601482), the Research Grants of Council of Hong Kong (C6009-17G, A-HKUST605/16, C2014-15G, N-HKUST604/14, and 16305015, 16301614), the Innovation of Technology Commission (ITC-CNERC14SC01 and ITS/254/17). This work was also technically supported by AIEgen Biotech Co., Ltd..

Conflict of interest

The authors declare no conflict of interest.

Keywords: aggregation-induced emission · bio-orthogonal chemistry · cancer · metabolic labeling · tumors

- [1] H. Kobayashi, P. L. Choyke, *Acc. Chem. Res.* **2011**, *44*, 83–90.
- [2] a) X. Shi, C. Y. Yu, H. Su, R. T. K. Kwok, M. Jiang, Z. He, J. W. Y. Lam, B. Z. Tang, *Chem. Sci.* **2017**, *8*, 7014–7024; b) Y. Wu, Z. Chen, P. Zhang, L. Zhou, T. Jiang, H. Chen, P. Gong, D. S. Dimitrov, L. Cai, Q. Zhao, *Chem. Commun.* **2018**, *54*, 7314–7317; c) Y. Cheng, C. Sun, X. Ou, B. Liu, X. Lou, F. Xia, *Chem. Sci.* **2017**, *8*, 4571–4578; d) H. Shi, Z. Tang, Y. Kim, H. Nie, Y. F. Huang, X. He, K. Deng, K. Wang, W. Tan, *Chem. Asian J.* **2010**, *5*, 2209–2213; e) P. Zhang, Z. Zhao, C. Li, H. Su, Y. Wu, R. T. K. Kwok, J. W. Y. Lam, P. Gong, L. Cai, B. Z. Tang, *Anal. Chem.* **2018**, *90*, 1063–1067.
- [3] M. Patra, K. Zarschler, H.-J. Pietzsch, H. Stephan, G. Gasser, *Chem. Soc. Rev.* **2016**, *45*, 6415–6431.
- [4] D. Baran, M. G. Pszolla, G. D. Lapidoth, C. Norn, O. Dym, T. Unger, S. Albeck, M. D. Tyka, S. J. Fleishman, *Proc. Natl. Acad. Sci. USA* **2017**, *114*, 10900–10905.
- [5] a) H. Wu, N. K. Devaraj, *Acc. Chem. Res.* **2018**, *51*, 1249–1259; b) F. Hu, D. M. Kenry, X. Cai, W. Wu, D. Kong, B. Liu, *Angew. Chem. Int. Ed.* **2018**, *57*, 10182–10186; *Angew. Chem.* **2018**, *130*, 10339–10343; c) D. Mao, F. Hu, D. M. Kenry, S. Ji, W. Wu, D. Ding, D. Kong, B. Liu, *Adv. Mater.* **2018**, *30*, 1706831; d) J.-S. Ni, P. Zhang, T. Jiang, Y. Chen, H. Su, D. Wang, Z.-Q. Yu, R. T. K. Kwok, Z. Zhao, J. W. Y. Lam, B. Z. Tang, *Adv. Mater.* **2018**, *30*, 1706831.
- [6] L. Xu, J. S. Josan, J. Vagner, M. R. Caplan, V. J. Hruby, E. A. Mash, R. M. Lynch, D. L. Morse, R. J. Gillies, *Proc. Natl. Acad. Sci. USA* **2012**, *109*, 21295–21300.
- [7] a) J. Du, M. A. Meledeo, Z. Wang, H. S. Khanna, V. D. P. Paruchuri, K. J. Yarema, *Glycobiology* **2009**, *19*, 1382–1401; b) H. Wang, R. Wang, K. Cai, H. He, Y. Liu, J. Yen, Z. Wang, M. Xu, Y. Sun, X. Zhou, Q. Yin, L. Tang, I. T. Dobrucki, L. W. Dobrucki, E. J. Chaney, S. A. Boppart, T. M. Fan, S. Lezmi, X. Chen, L. Yin, J. Cheng, *Nat. Chem. Biol.* **2017**, *13*, 415–424; c) H. Y. Yoon, M. L. Shin, M. K. Shim, S. Lee, J. H. Na, H. Koo, H. Lee, J.-H. Kim, K. Y. Lee, K. Kim, I. C. Kwon, *Mol. Pharm.* **2017**, *14*, 1558–1570.
- [8] P. Q. Nguyen, N.-M. D. Courchesne, A. Duraj-Thatte, P. Praveschotinunt, N. S. Joshi, *Adv. Mater.* **2018**, *30*, 1704847.
- [9] a) L. Du, H. Qin, T. Ma, T. Zhang, D. Xing, *ACS Nano* **2017**, *11*, 8930–8943; b) S. Lee, H. Koo, J. H. Na, S. J. Han, H. S. Min, S. J. Lee, S. H. Kim, S. H. Yun, S. Y. Jeong, I. C. Kwon, K. Choi, K. Kim, *ACS Nano* **2014**, *8*, 2048–2063.
- [10] a) Q. Miao, C. Xie, X. Zhen, Y. Lyu, H. Duan, X. Liu, J. V. Jokerst, K. Pu, *Nat. Biotechnol.* **2017**, *35*, 1102–1110; b) X. Gao, Y. Cui, R. M. Levenson, L. W. K. Chung, S. Nie, *Nat. Biotechnol.* **2004**, *22*, 969–976; c) K. Shou, Y. Tang, H. Chen, S. Chen, L. Zhang, A. Zhang, Q. Fan, A. Yu, Z. Cheng, *Chem. Sci.* **2018**, *9*, 3105–3110; d) I. Martinić, S. V. Eliseeva, S. Petoud, *J. Lumin.* **2017**, *189*, 19–43.
- [11] a) Y. Wang, R. Hu, G. Lin, I. Roy, K.-T. Yong, *ACS Appl. Mater. Interfaces* **2013**, *5*, 2786–2799; b) F. M. Winnik, D. Maysinger, *Acc. Chem. Res.* **2013**, *46*, 672–680; c) K. Li, B. Liu, *Chem. Soc. Rev.* **2014**, *43*, 6570–6597.
- [12] a) K. Li, Z. Zhu, P. Cai, R. Liu, N. Tomczak, D. Ding, J. Liu, W. Qin, Z. Zhao, Y. Hu, X. Chen, B. Z. Tang, B. Liu, *Chem. Mater.* **2013**, *25*, 4181–4187; b) J. Qi, C. Sun, A. Zebibula, H. Zhang, R. T. K. Kwok, X. Zhao, W. Xi, J. W. Y. Lam, J. Qian, B. Z. Tang, *Adv. Mater.* **2018**, *30*, 1706856; c) J. Qian, B. Z. Tang, *Chem* **2017**, *3*, 56–91; d) J. Mei, Y. Hong, J. W. Y. Lam, A. Qin, Y. Tang, B. Z. Tang, *Adv. Mater.* **2014**, *26*, 5429–5479.
- [13] Z. Zhao, H. Su, P. Zhang, Y. Cai, R. T. K. Kwok, Y. Chen, Z. He, X. Gu, X. He, H. H. Y. Sung, I. D. Willimas, J. W. Y. Lam, Z. Zhang, B. Z. Tang, *J. Mater. Chem. B* **2017**, *5*, 1650–1657.
- [14] N. Gulia, B. Pigulski, S. Szafert, *Organometallics* **2015**, *34*, 673–682.

Manuscript received: November 14, 2018

Revised manuscript received: December 3, 2018

Version of record online: December 21, 2018